Materials Chemistry and Physics 145 (2014) 186–196

Contents lists available at ScienceDirect

Materials Chemistry and Physics

journal homepage: www.elsevier.com/locate/matchemphys

A design of gradient interphase reinforced by silanized graphene oxide and its effect on carbon fiber/epoxy interface

Lei Chen, Hao Jin, Zhiwei Xu*, Mingjing Shan, Xu Tian, Caiyun Yang, Zhen Wang, Bowen Cheng

Key Laboratory of Advanced Braided Composites, Ministry of Education, School of Textiles, Tianjin Polytechnic University, Tianjin 300160, People's Republic of China

HIGHLIGHTS

- Graphene oxide was covalently functionalized with silane coupling agents.
- Gradient interphase composed of SGO and epoxy was designed in fiber/matrix.
- A new stiffness phase between fiber and matrix was found by AFM in force mode.
- Interfacial properties of composites containing SGO/epoxy interphase were increased.

GRAPHICAL ABSTRACT

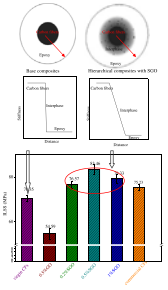

ARTICLE INFO

Article history:
Received 1 November 2013
Received in revised form
23 January 2014
Accepted 4 February 2014

Keywords:
Composite materials
Interfaces
Coatings
Atomic force microscopy
Mechanical properties

ABSTRACT

To improve the stress transfer and distribution of carbon fiber/epoxy interface, a gradient interphase reinforced by graphene oxide (GO) was designed in the composites. GO was introduced onto the surface of carbon fibers by physical adsorption, forming a gradient interphase in composite interface during the procedure of resin wetting. In order to improve the dispersion of GO in gradient interphase and chemical adhesion between GO and epoxy, GO was covalently functionalized with silane coupling agents and the silanized graphene oxide (SGO) was introduced into the gradient interphase as well. Compared with the base composites without nanosheets, the interfacial shear strength (IFSS), interlaminar shear strength (ILSS), flexural and tensile properties of hierarchical composites decreased seriously when 0.5 wt% GO was introduced on carbon fiber surface. However, hierarchical composites containing 0.5 wt% SGO showed a significant increase 60% in IFSS, 19% in ILSS, 15% in flexural strength and 16% in flexural modulus. A new stiffness phase between carbon fibers and matrix was found in the stiffness distribution curve of hierarchical composites by atomic force microscope in force mode. In addition, the stiffness of interphase was proved to change gradually from carbon fibers to epoxy, indicating the gradient dispersion of nanosheets in interphase.

1. Introduction

Carbon fiber/epoxy composites with their favorable strength-to-weight and stiffness-to-weight ratios are replacing traditional metallic materials in a wide range of applications [1–3], such as aeronautical and astronautical structures (e.g., aircraft, space

* Corresponding author. Tel./fax: +86 22 24528258.
E-mail address: xuzhiwei@tjpu.edu.cn (Z. Xu).

http://dx.doi.org/10.1016/j.matchemphys.2014.02.001
0254-0584/

shuttle, and satellite), ground vehicles and sports utilities [4–6]. The performance of carbon fiber/epoxy composites is, to a large extent, influenced by the interfacial properties. Good interfacial properties are essential to ensure the efficient load transfer from matrix to fillers, which help to reduce stress concentrations and improve overall mechanical properties [7,8].

Recently, much effort was focused on assembling carbon nanotubes onto carbon fibers to improve the interfacial properties of composites due to consuming energy by pulling out carbon nanotubes from the matrix or breakage of carbon nanotubes [9–14]. In addition, multiscale reinforcements, containing fibers together with graphenes in the matrix or on the surface of fibers, can enhance the interface properties (e.g., fatigue life) of carbon fiber/epoxy composites [15]. Graphene oxide (GO), bearing oxygen functional groups on its basal planes and edges, is a single layer of graphite oxide and exhibits excellent performance [16–19]. It has been demonstrated that the interfacial and tensile properties of carbon fiber/epoxy composites were enhanced by using fiber sizing with GO sheets [8]. However, the exact improvement mechanisms of interfacial properties were not clear.

Herein, a simple and effective method of designing a gradient interphase could improve the stress transfer and distribution of composite interface. This interphase in the composites learns from the bio-logical systems, which rarely exhibit discrete boundaries between two materials with vastly different mechanical properties [20]. In this work, GO was introduced onto the surface of carbon fibers and a gradient interphase with modulus between fibers and matrix [21,22] could be formed in the composite interface. However, the homogeneous dispersion and efficient chemical bonding with epoxy are the main challenges due to the strong tendency to aggregation of GO [23]. Fortunately, the tunable oxygenous functional groups of GO facilitate the modification on the surface [24–27]. In order to improve the dispersion of GO in gradient interphase and chemical adhesion between GO and epoxy, GO was covalently functionalized with silane coupling agents. It is expected that covalent functionalization of GO not only makes the dispersibility of GO better but also enables the interfacial interactions between GO and matrix stronger [28].

In this study, GO was modified with silane coupling agent KH-550 (3-Aminopropyltriethoxysilane) to improve the dispersion of GO in gradient interphase and chemical adhesion between GO and epoxy. Functional groups and chemical elements of silanized graphene oxide (SGO) were examined by Fourier Transform Infrared Spectroscopy (FTIR) and X-ray photoelectron spectroscopy (XPS). The surface topography of carbon fibers and the distribution of GO and SGO sheets on carbon fiber surface were detected by scanning electron microscope (SEM). The gradient interphase reinforced by GO or SGO was formed between carbon fibers and epoxy. The interlaminar shear strength (ILSS) and flexural properties of these composites were evaluated by three-point short beam shear tests and flexural tests. In view of interface width typically ranging from a few micrometers to several hundred nanometers, it seemed that nanomechanical technique such as atomic force microscope (AFM) was an adequate to characterize the local mechanical properties within this region [29]. Information about the changes in local stiffness within the interfacial region could be delivered by AFM in force mode [20,30].

2. Experiment section

2.1. Materials

Commercially available T700S carbon fibers (12 K, 1.78 g cm^{-3}), purchased from Japan Toray, were used as reinforcing fillers in the present work. Epoxy (HS5382) based on bisphenol-A with an epoxy value of 0.45–0.50 was obtained from Guangdong Hai Xu Resin Factory, China. The curing agent, tetrahydrophthalic anhydride was purchased from Wenzhou Qingming Chemical, China. Graphite powders with an average diameter of 10 μm were purchased from Qingdao AoKe ShiMoCo. Ltd., China. *N*,*N*′-dicyclohexyl-carbodiimide (DCC, 99%), silane coupling agent KH-550, acetone, hydrochloric acid, potassium permanganate and concentrated sulfuric acid were purchased from Tianjin chemical factory and used as received.

2.2. Preparation and silanization of GO

Graphite oxide was prepared using an improved Hummers method [31,32]. A 9:1 mixture of concentrated H_2SO_4/H_3PO_4 (360:40 ml) was added to a mixture of graphite powders (3.0 g, 1 wt equiv) and $KMnO_4$ (18.0 g, 6 wt equiv), producing a slight exotherm to 35–40 °C. The mixture was stirred for 12 h at 50 °C, forming a thick paste. Subsequently, it was cooled to room temperature and poured onto ice (400 ml) with 30% H_2O_2 (3 mL). The remaining solid materials were then washed in succession with deionized water until pH was 7. At last, they were dried at vacuum freeze drier for 12 h to get graphite oxide.

GO nanosheets containing hydroxyl and epoxide functional groups on their basal planes, carboxyl and carbonyl groups on the edges reacted with silanol of silane coupling agent KH-550 [23]. Briefly, graphite oxide (35 mg) was dispersed in deionized water (100 ml) and treated by ultrasonication for 2 h, forming homogeneous GO solution. Then silane coupling agent KH-550 (10 ml) was added into the brown and homogeneous mixture, stirred and heated to 70 °C for 24 h. After that, the resulting black and homogeneous SGO sheets were centrifuged. Then they were washed by a large amount of absolute ethanol and deionized water until the pH value of filtrate reached 7 in order to remove the residual silane coupling agent. At last, the materials were dried 24 h at 50 °C under vacuum.

2.3. Introduction of GO and SGO on carbon fiber surface

At first, T700S carbon fibers (12 K, 1.78 g cm^{-3}) were refluxed into acetone for 12 h and petroleum ether for another 12 h to exclude the possible effects of commercial sizing from the improvement of ILSS and flexural properties in the system. Then GO and SGO were dispersed in deionized water and acetone, and sonicated for 2 h respectively to form a suspension 3 mg ml^{-1}. After that, the virgin carbon fibers which have been weighed were soaked in the homogeneous mixtures for 20 s to absorb the solutions containing carbon nanoparticles. Then these carbon fibers coated by carbon nanoparticles were dried at 50 °C under vacuum and the weight of carbon fibers was measured again. The weight of carbon nanoparticles was calculated by changes in weight of carbon fibers. Then these steps were repeated until the contents of carbon nanoparticles in composites reached 0.2 wt%, 0.5 wt%, 1 wt%.

2.4. Fabrication of composite samples

Preparation of carbon fiber composites was done following the protocol: (1) The prepared undirectional carbon fibers were put into the grooves of mold, and the volume percent of carbon fibers was kept the same in different batches. (2) Epoxy with 70 wt% curing agent and 1 wt% 2-ethyl-4-methylimidazole was mixed and degassed under vacuum. (3) The prepared epoxy was injected into the mold by resin transfer molding (RTM) method. (4) The mold was put into oven to cure the composites, and followed by a post-curing step at 90 °C for 2 h and at 120 °C for 2 h and 150 °C for 4 h. (5) After curing, the samples were cooled naturally to room

temperature. The final fiber volume fraction of undirectional composite strips was calculated in the range from 50 to 55%. The strips with dimensions of 250 mm × 10 mm were prepared for the three-point short beam shear tests and flexural tests.

2.5. Characterizations

AFM observation of GO, SGO and composites was performed on a CSPM 5500 scanning probe microscope. GO dispersed in water and SGO dispersed in acetone were dip-coated onto freshly cleaved mica surfaces before testing. The composite fracture surface was ground, polished and washed. XPS was carried out with a VG Escalab Mark II spectrometer (Thermo-VG Scientific Ltd. UK), using Al Ka excitation radiation (ht = 1253.6 eV). FTIR spectra were recorded using a Nicolet 6700 spectrophotometer in KBr pellets. SEM images of surface topography of carbon fibers and fracture surface of composite specimens were obtained on a Hitachi S-4800 field-emission SEM system (operated at 4 kV). The samples were coated with a conductive layer of gold.

A microbond test was carried out using an interfacial microbond evaluation instrument made by East Japan, LTD. The fiber was loaded at a speed of 1 μm s^{-1} from the matrix while the force was recorded against the displacement using a computer. Three-point short beam shear tests and flexural tests were carried out to determine the effect of GO and SGO on the interface properties of the unidirectional carbon fiber/epoxy composites, according to the JC/T773-2010 standards and ASTM D 790M, respectively. The short-beam specimens (20 mm in length, 10 mm in width, and 2.4 mm in thickness) and flexural specimens (50 mm in length, 10 mm in width, and 2.4 mm in thickness) were cut from the composites by using a water-cooled diamond saw. The short-beam shear tests were performed in an Instron (3369, USA) using a cross-head speed of 2 mm min^{-1}. The three-point flexural tests with a support span of 38.4 mm were used to fracture the specimens on the same Instron mechanical testing machine. The constant strain rate (0.01 mm mm^{-1} min^{-1}) was maintained. The tensile tests of composites were performed by using an Instron (3369, USA) according to ASTM D3039, with a cross-head speed of 2 mm min^{-1}. The specimens were cut to size of 250 mm × 15 mm × 1.0 mm with four end-tabs bonded to both ends (aluminum tab with dimensions of 50 mm × 15 mm × 1.0 mm). DMA tests were carried out on a dynamic mechanical thermal analyzer (MettlerToledo 861e instrument) operating in the three-point bending mode at a frequency of 1.0 Hz. Specimen dimensions were 40 mm × 6 mm × 2.5 mm. The temperature range was 25–200 °C with a heating rate of 3 °C min^{-1}.

3. Results and discussion

3.1. Architecture, composition and dispersion of GO and SGO

AFM observation of GO dispersion in water after their deposition on a freshly cleaved mica sheet through drop-casting was carried out. A representative AFM image of GO was shown in Fig. 1(a), which revealed the presence of GO irregularly shaped with uniform

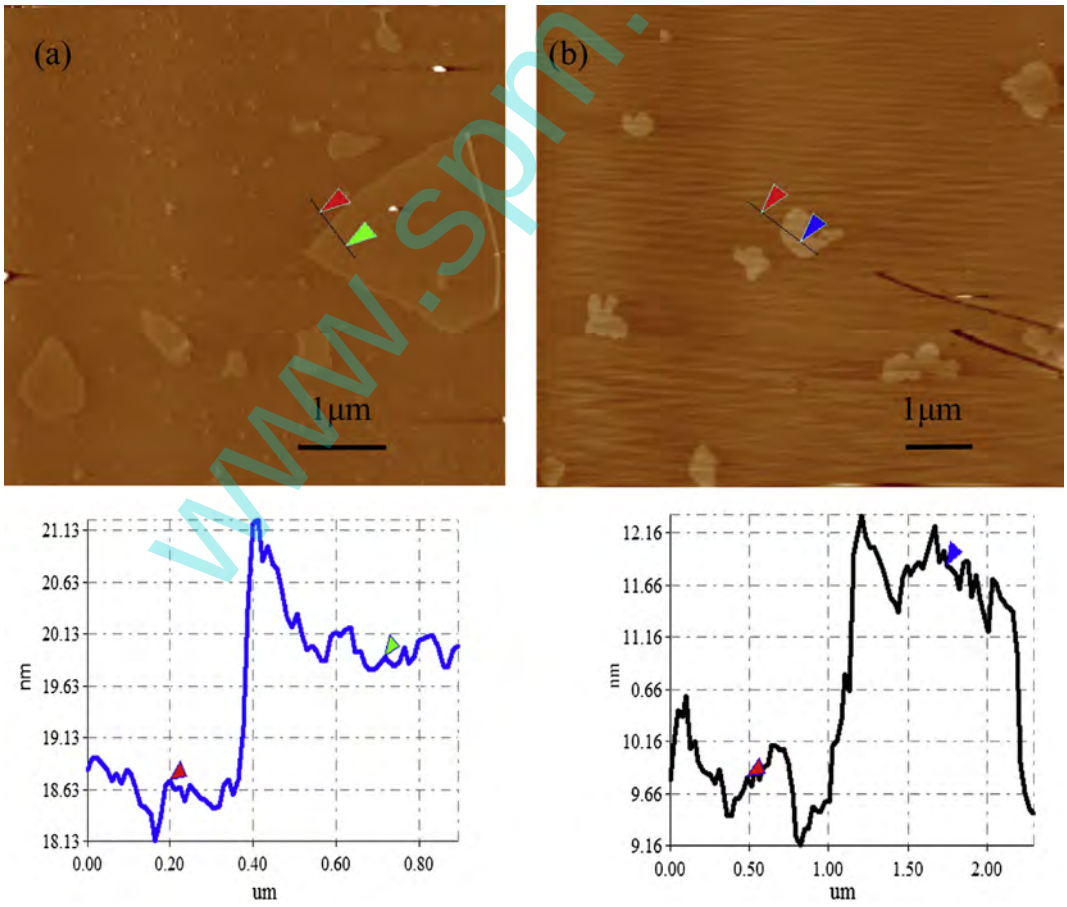

Fig. 1. (a) AFM image of GO dispersion in water on freshly cleaved mica surface through drop-casting, and height profile (below) along the blue line indicating a sheet thickness of about 1.2 nm. (b) AFM image of SGO dispersion in acetone on freshly cleaved mica surface through drop-casting, and height profile (below) along the blue line indicating a sheet thickness of about 2.1 nm. (For interpretation of the references to color in this figure legend, the reader is referred to the web version of this article.)

thickness 1.2 nm, which was in good agreement with previous reported single-layer [17]. Fig. 1(b) indicated that the average thickness of SGO was around 2.1 nm, which was thicker than that of GO. The increase of SGO in thickness was attributed to the presence of functionalized silane chains grafted on GO. In addition, the width of SGO decreased in comparison to GO due to the chemical reaction with silane coupling agent. The results were in agreement with the literature [23].

Fig. 2 illustrated the synthesis process of covalent interaction between GO and silane coupling agent KH-550. GO contained hydroxyl and epoxy functional groups on its edges and basal planes, which could dehydrate with silane coupling agents in the presence of catalyst [23,28,33,34]. On one hand, GO contained hydroxyl functional groups on its basal planes and edges, which could provide the active sites to react with silanol of silane coupling agents after hydrolysis [23,34]. On the other hand, the epoxy groups of GO could react with amino groups of silane coupling agents [28]. GO can be dispersed into water, forming stable and homogeneous dispersions by ultrasonication as shown in Fig. 2. After reacting with silane coupling agents, the resulting black SGO can be dispersed in acetone homogeneously instead of water.

FTIR spectra of GO and SGO were presented in Fig. 3. The results from FTIR revealed that the characteristic band of carboxyl groups in GO appeared at 1702 cm^{-1}. After interacting with silane coupling agent, the doublet at 2930 and 2850 cm^{-1} corresponding to symmetric and asymmetric vibration of $-CH_2-$ groups appeared, which was assigned to the alkyl chains for the silane moieties of SGO [23]. Moreover, the appearance of bands at 1059 and 936 cm^{-1} (Si–O–C/Si–O–Si) provided more evidence for this successful chemical functionalization [28]. In addition, the N–H vibration in amino groups expected at around 3300 cm^{-1} was present. The results indicated that GO was reacted with silane coupling agent successfully.

XPS analysis was employed to elucidate the surface composition of GO and SGO, which could provide more information of the interactions between GO and silane coupling agent. The high resolution XPS spectra in the C1s region of (a) GO and (b) SGO were

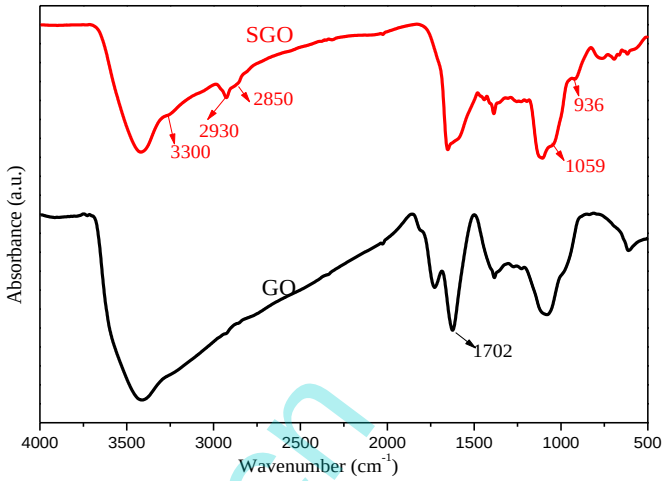

Fig. 3. FTIR spectra of GO and SGO.

presented in Fig. 4. Fig. 4(a) clearly demonstrated that GO had a considerable degree of oxidation with four peaks appearing at 284.8, 286.4, 287.1 and 288.1 eV, which could be ascribed to the non-oxygenated ring C atoms, the C atoms in hydroxyl groups, the C atoms in epoxy/ether groups, and the carbonyl C structure, respectively [23,33,35]. The C1s XPS spectrum of SGO (Fig. 4(b)) also exhibited these same oxygen functionalities, however, the peak intensities of oxygenated C in hydroxyl and epoxy/ether groups dramatically decreased, and an additional component at 286.0 eV assigning to C bound to nitrogen appeared owing to the reaction with silane coupling agent. In addition, the peak intensities of carbonyl C structure in SGO decreased seriously compared with GO as a result of the decomposition of carbonyl at reaction temperature (70 °C). The high resolution XPS spectra in the O1s region of GO and SGO were shown in Fig. 4(c), and the O1s in GO appeared at 532.9 eV, assigning to O in C–O–C, C–O–H and C=O [28]. After

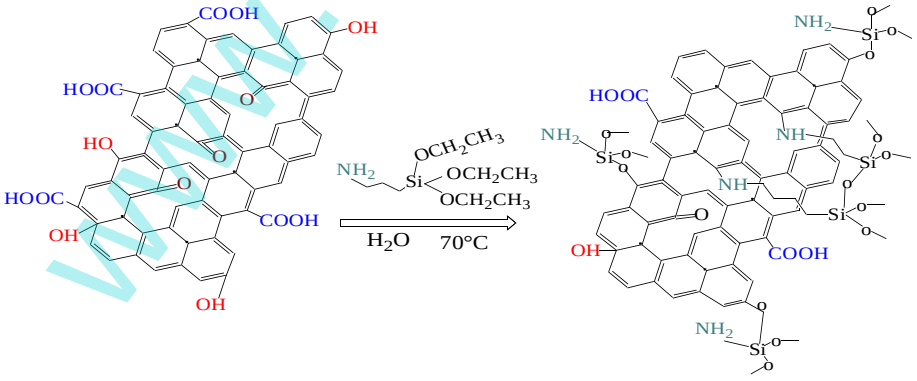

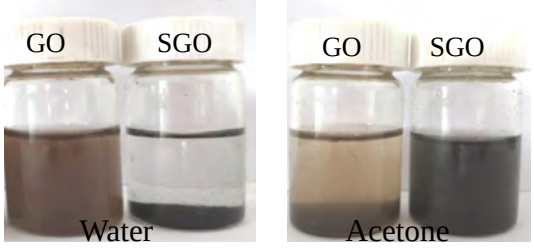

Fig. 2. Illustration of the reaction between GO and silane coupling agent, and photographs of GO and SGO dispersed in water and acetone.

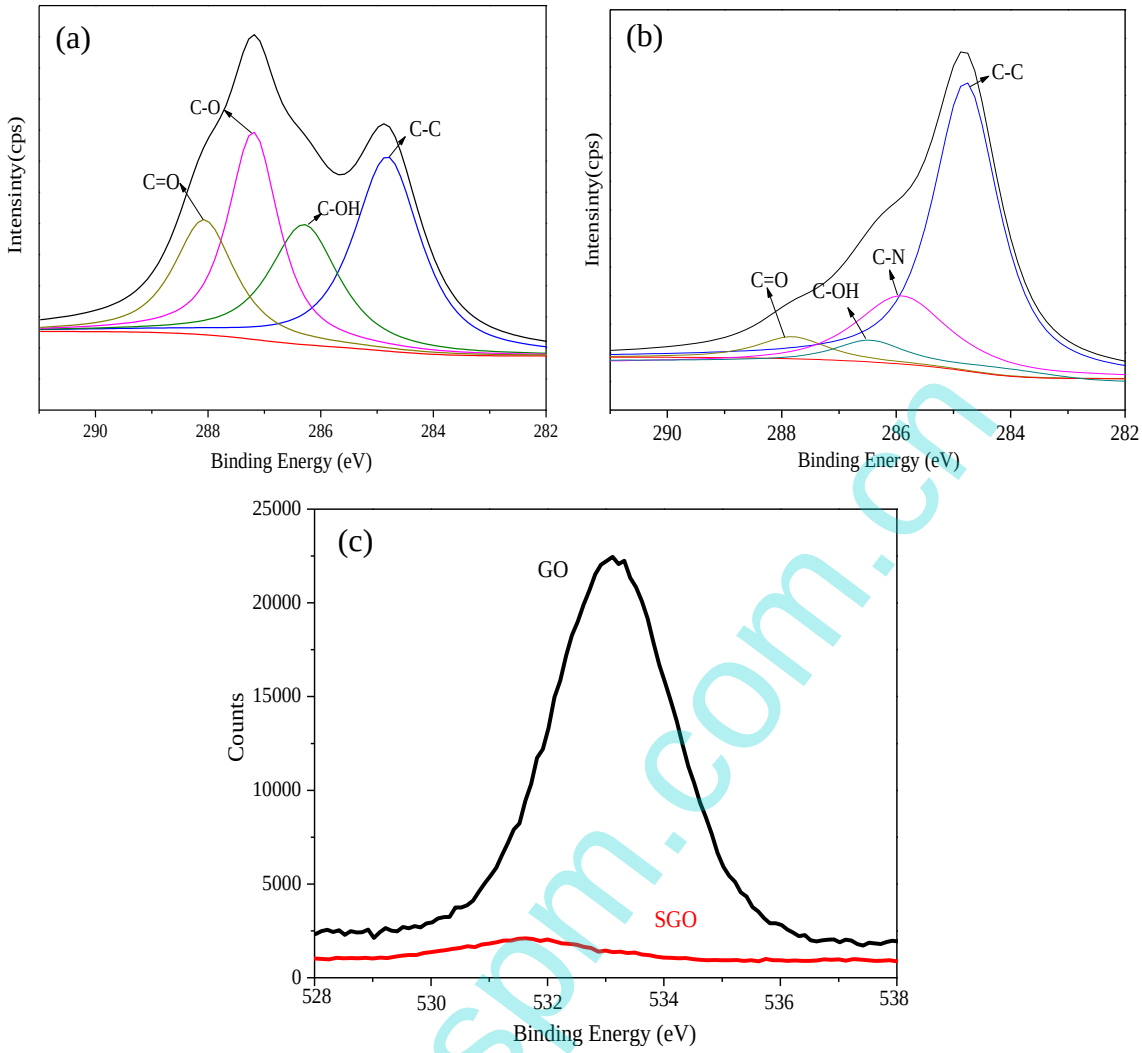

Fig. 4. High resolution C1s XPS spectra of (a) GO, (b) SGO, and (c) high resolution O1s XPS spectra of GO (black) and SGO (red).

interaction with silane coupling agent, the peak intensities of O1s decreased seriously and removed to 531.8 eV, which was assigned to O in C–O–Si/Si–O–Si, and C=O. As can be seen from Table 1, the N and Si element concentration of SGO showed a significant increase compared with GO. This increase of Si and N elements was originated from silane coupling agent, suggesting the successful covalent functionalization.

3.2. Surface topography and element analysis of carbon fibers

The changes of surface topography and element for carbon fibers after different treatments were verified by SEM, and the results were shown in Fig. 5. Smooth surface with slight convex hills of commercial fiber T700S was shown in Fig. 5(a). After removing the commercial sizing, the surface of carbon fibers became much smoother as shown in Fig. 5(b). In addition, the oxide element of virgin carbon fibers decreased seriously compared with the commercial fiber, indicating successful clearing of commercial sizing as shown in Fig. 5(c) and (d). Fig. 5(e) and (f) showed the surface topographies of carbon fibers absorbed with GO and SGO, respectively. GO was lapped on carbon fibers like a blanket according to electrostatic adsorption principle. However, SGO with smaller width was leaned on carbon fibers out of order.

Table 1
Atomic concentration table of GO and SGO.

Sample	C	O	N	Si
GO	62.67%	37.13%	0%	0%
SGO	68.29%	21.34%	5.05%	5.32%

3.3. Mechanical properties of composites

3.3.1. IFSS and ILSS of carbon fiber/epoxy

IFSS results of each carbon fiber type could be seen in Fig. 6, it was clearly demonstrated that the presence of SGO sheets surrounding the fiber contributed to the improvement of IFSS. What's more, it was found that the IFSS of SGO modified carbon fibers was much higher than that of commercial-sized carbon fiber, especially carbon fibers containing 0.5 wt% SGO yielding IFSS of 64.8 MPa, which had an increase of about 60% compared with virgin carbon fibers and about 50% in comparison to commercial-sized carbon fiber. The results might be related to the fact that the SGO/epoxy interphase could transfer stress, absorb energy and prevent the crack propagation effectively. When the content was lower than 0.5 wt%, the SGO sheets were surrounding on the fiber surface homogeneously, whereas further increasing SGO loading from 0.5 to 1 wt% led to the decrease of IFSS due to the agglomeration of

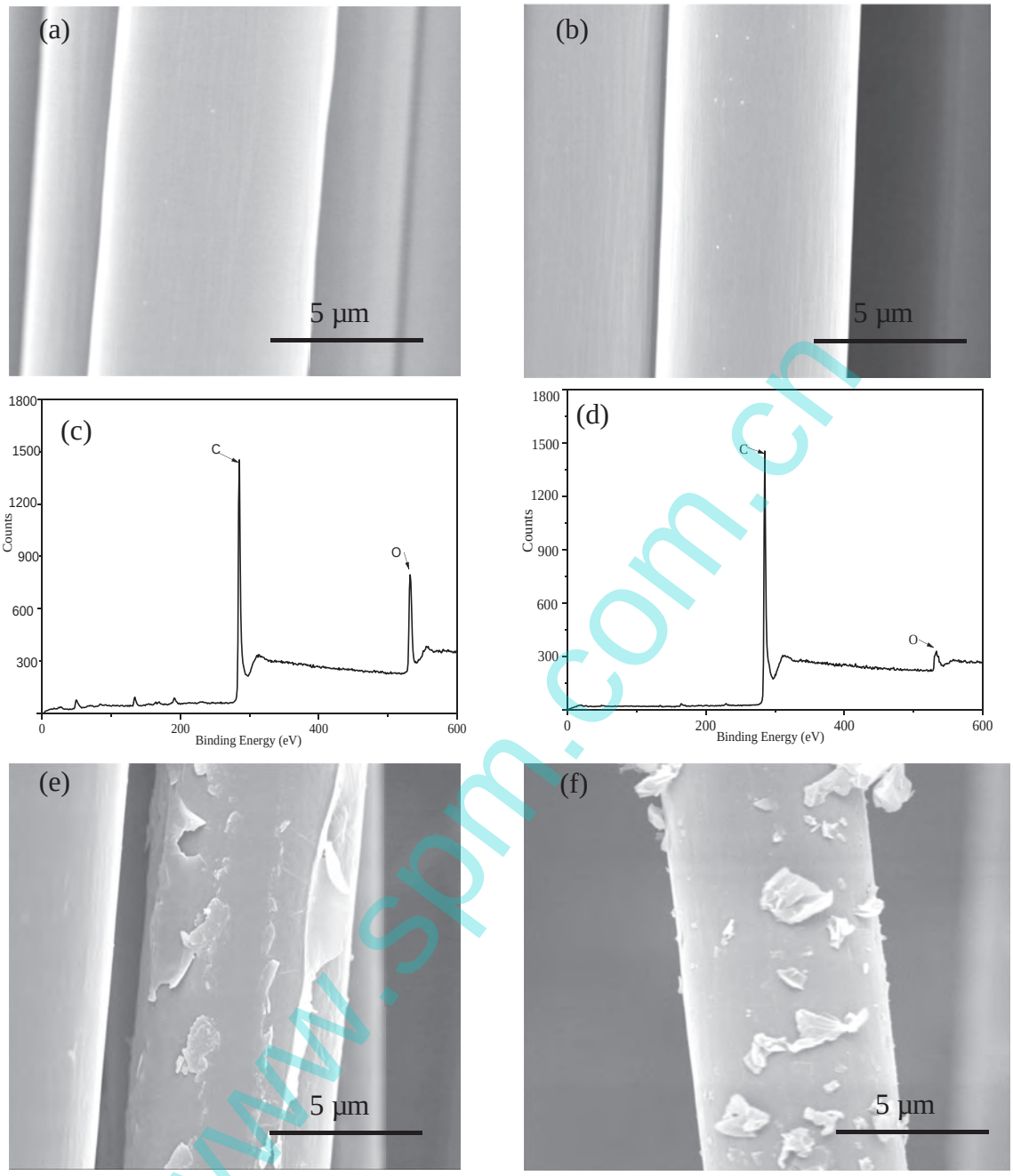

Fig. 5. SEM images of (a) T700 carbon fibers, (b) virgin carbon fibers, (c) and (d) XPS survey scans of T700 carbon fibers and virgin carbon fibers, (e) virgin carbon fibers with GO, and (f) virgin carbon fibers with SGO.

excessive SGO in the interphase region. However, the IFSS of carbon fibers containing 0.5 wt% GO decreased seriously compared with the base composites. The results might be due to the fact that GO with large size weakened the wettability between carbon fibers and matrix and the epoxy could be stripped from carbon fibers easily in failure mode.

ILSS is one of the most important interfacial properties for carbon fiber/epoxy composites. To better understand the relationship between the gradient interphase microstructure and interfacial properties, three-point short beam shear method was used to evaluate the ILSS of composites. As shown in Fig. 7, after removing the commercial sizing, the ILSS of the base composites decreased compared with the commercial carbon fiber/epoxy composites owing to poor interfacial adhesion between carbon fibers and epoxy. The ILSS of hierarchical composites containing 0.5 wt% GO (54.59 ± 2.3 MPa) decreased by 23% in comparison to the base composites (70.35 ± 1.8 MPa), which was attributed to the GO agglomeration and poor chemical adhesion between GO and epoxy. As a result, the gradient interphase composed of GO and epoxy could not transfer the load effectively, and the ILSS of composites was weakened by the influence of stress distribution and fracture behavior of interface. In addition, GO with large size absorbed on carbon fibers hindered the resin wetting during RTM, leading to poor adhesion between carbon fibers and epoxy. Consequently, the interfacial adhesion of hierarchical composites with GO was weaker than that of the base composites, resulting in the decrease of ILSS.

Hierarchical composites with 0.5 wt% SGO was measured to have a maximum ILSS (83.46 ± 2.1 MPa), with an increase of 19% as

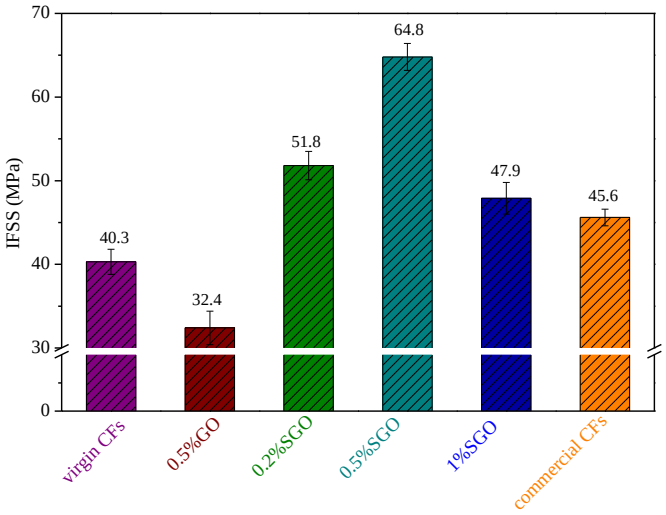

Fig. 6. IFSS of carbon fiber/epoxy composites with nanosheets.

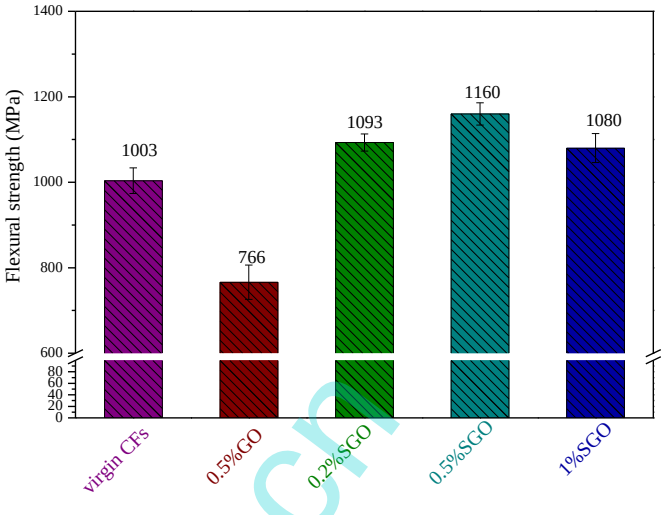

Fig. 8. Flexural strength of carbon fiber/epoxy composites with nanosheets.

compared with the base composites, which was at a relatively high level of improvement for the hybrid reinforced composites in the literature. The results indicated that the gradient interphase composed of SGO and epoxy contributed to the measured improvement in interfacial properties. What's more, the chemical adhesion between SGO and epoxy was enhanced owing to the fact that the amino-groups of silane coupling agents can be chemically interacted with epoxy. However, the ILSS value of hierarchical composites with 1 wt% SGO (79.33 ± 1.5 MPa) decreased in comparison to hierarchical composites with 0.5 wt% SGO. This might be due to the agglomeration of excessive SGO in the interphase, which affected the microstructure of gradient interphase.

3.3.2. Flexural properties

Based on the experimental load–deflection curves, the flexural strength and flexural modulus of composites could be extracted (Figs. 8 and 9). The results indicated that the flexural strength and flexural modulus of hierarchical composites containing GO were all decreased seriously upon impregnation of GO into the composites. However, the flexural strength and flexural modulus of hierarchical composites containing SGO were increased compared with base composites. Moreover, hierarchical composites containing 0.5 wt% SGO showed the highest increase of 15% in flexural strength and 16% in flexural modulus. The gradient interphase composed of SGO and epoxy was proved to be contributed to the improvement in interfacial properties. The modulus of hierarchical composites containing SGO was increased upon impregnation of SGO into the composites. This would dissipate the strain energy, prevent the failure of composites and lead to a higher value of work of fracture. However, the flexural strength and flexural modulus of hierarchical composites with 1 wt% SGO were decreased in comparison to the hierarchical composites with 0.5 wt% SGO. The results might be related to the fact that the excess SGO which were agglomerated on carbon fiber surface and the interfacial region became stress concentration sites, resulting in deterioration of flexural properties.

3.3.3. Tensile properties

To further inspect the enhancing effect of GO and SGO, we investigated the tensile properties of carbon fiber/epoxy composites. The results of tensile tests could be seen in Table 2. It was clearly verified that the tensile strength of hierarchical composites containing 0.5 wt% GO was lower than that of the base composites. For elastic modulus and elongation of hierarchical composites containing GO, there was serious decrease observed in comparison

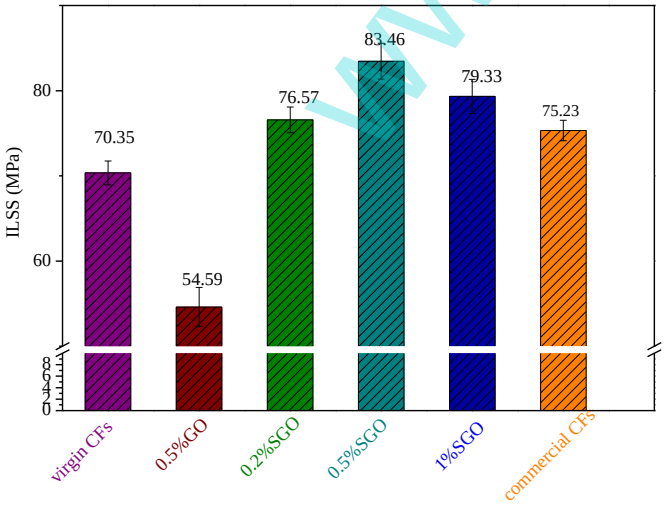

Fig. 7. ILSS of carbon fiber/epoxy composites with nanosheets.

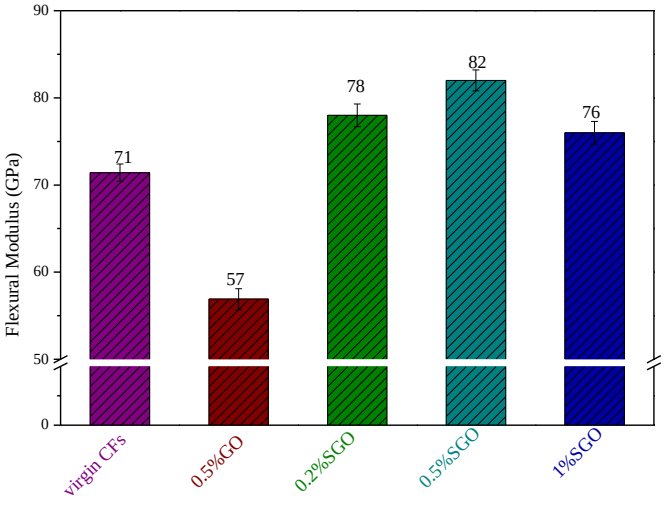

Fig. 9. Flexural modulus of carbon fiber/epoxy composites with nanosheets.

Table 2
Tensile results of composites tested in fiber longitudinal direction.

Sample	Tensile strength (MPa)	Elastic modulus (GPa)	Elongation (%)
Base composites	1340 ± 52	40.5 ± 2.0	1.78 ± 0.3
Composites with GO	1150 ± 60	34.2 ± 1.5	1.46 ± 0.2
Composites with SGO	1543 ± 48	48.7 ± 1.4	2.13 ± 0.5

to that of the base composites, showing a similar trend to the tensile strength. However, hierarchical composites containing 0.5 wt% SGO showed 15% increased in tensile strength, 20% in elastic modulus and 19% in elongation compared with the base composites. The tensile properties of carbon fiber/epoxy composites were in general dominated by the fiber behavior, but it has been demonstrated that the tensile properties of fibers could be affected by introducing nanoparticles in fiber coating or surface [8,20]. Due to the GO agglomeration and poor chemical adhesion between GO and epoxy, micro cracks propagation increased at the gradient interphase. Thus, tensile properties started to come down as interface could not act as effective load transfer medium between fibers and matrix. However, stress transfer, energy absorption and prevention of crack propagation could be improved by the SGO/epoxy gradient interface, which enhanced the tensile properties eventually.

3.3.4. Viscoelastic/thermo-mechanical properties

The mechanical properties of composites under dynamic load were characterized by DMA, which could observe carbon fiber/epoxy samples stiffness behavior as a function of temperature and analyze the effect of GO and SGO on thermo-mechanical performance. The variations of the storage modulus (E_0) and the damping (tan δ) with temperature for the composites reinforced by different carbon fibers are shown in Figs. 10 and 11. The results indicated that E_0 for hierarchical composites containing SGO was higher than that of the base composites. As shown in Fig. 10, E_0 increased from 33 to 40 GPa below glass transition temperature (T_g) and from 8 to 11 GPa above T_g. The presence of SGO enabled the hierarchical composites to sustain stiffness at higher temperature near T_g. This may be due to the better interfacial adhesion between matrix and reinforcements, which can bring an increase in the volume fraction of interphase in the composites and a decrease in the effective polymer chain mobility at the interphase region [36]. This interphase area could work as an additional reinforcement for mechanical

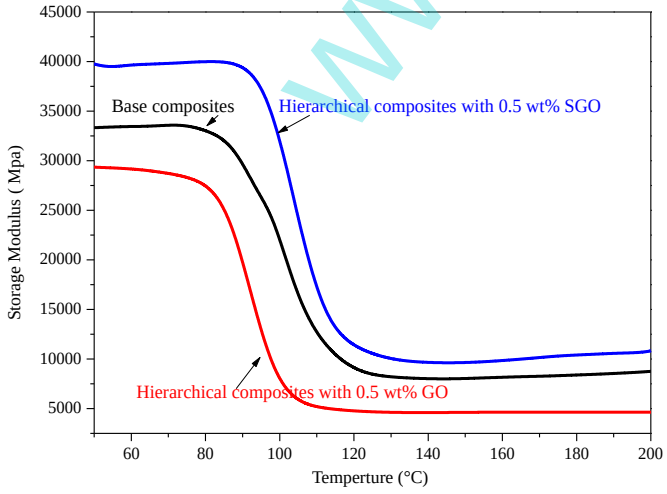

Fig. 10. Storage modulus vs. temperature response of composites.

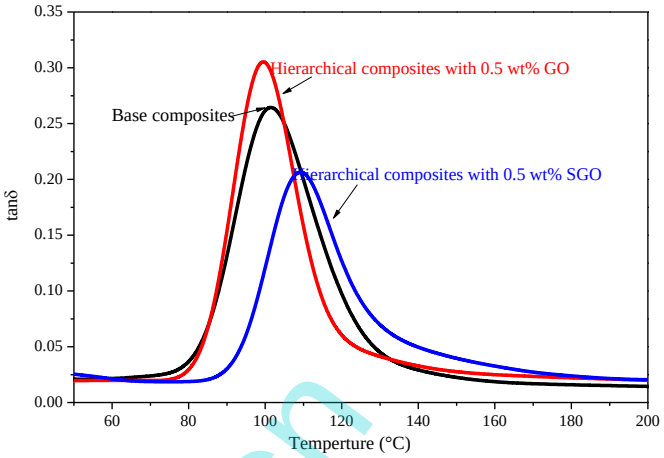

Fig. 11. Tan δ vs. temperature response of composites.

stiffening of the composites [20]. However, E_0 for hierarchical composites containing GO decreased compared with the base composites. The results were in agreement with the flexural modulus.

T_g was identified as a maximum in the tan δ curves. The untreated fiber composites had a T_g of 100 °C. T_g of hierarchical composites containing GO shifted toward lower temperature and hierarchical composites containing SGO shifted toward higher temperature, about 3 °C lower and 9 °C higher than that of the untreated ones. The damping (tan δ) of hierarchical composites containing GO increased and hierarchical composites containing SGO decreased. The decrease of T_g and increase of damping (tan δ) for composites reinforced by GO may be related to the fact that the GO agglomerated in the interphase region could alter the flow behavior of epoxy, which resulted in nano-meter scale porosities [37]. As a result, free volume might be created due to these porosities between polymer molecules which facilitated in polymer chain motion [10]. So these might be the reasons for drop in glass transition temperature and rise in damping of carbon fiber/epoxy containing 0.5 wt% GO. The increase of T_g and decrease of damping (tan δ) for carbon fiber/epoxy containing 0.5 wt% SGO probably might be due to the enhancement of a restricted mobility interphase region composed of SGO and epoxy [38].

3.4. Element and stiffness distribution of gradient interphase

In view of interface width typically ranging from a few micrometers to several hundred nanometers, AFM in force mode was used to characterize the local stiffness. Fig. 12(a) was the illustration of base composites and Fig. 12(b) was the illustration of composites stiffness along the direction of arrow in Fig. 12(a). The stiffness value of carbon fibers was much higher than that of epoxy. Therefore, the change of stiffness varying from carbon fibers to epoxy was very sharp. Fig. 12(c) was SEM image of fracture surface of the base composites. Fig. 12(d) was the carbon element content varying from carbon fibers to epoxy corresponding to Fig. 12(c) delivered by SEM/energy dispersive spectrometer (EDS). Fig. 12(e) showed the relative stiffness images of cross-section areas in the base composites by AFM in force mode. The relative stiffness image of carbon fibers was brighter than the surrounding epoxy, which meant that the stiffness of carbon fibers was higher than epoxy. It demonstrated that the relative stiffness image displayed a clear distinction between carbon fibers and the surrounding epoxy in Fig. 12(e). Fig. 12(f) was the corresponding relative stiffness distribution curve of cross-section areas of Fig. 12(e). The abscissa of

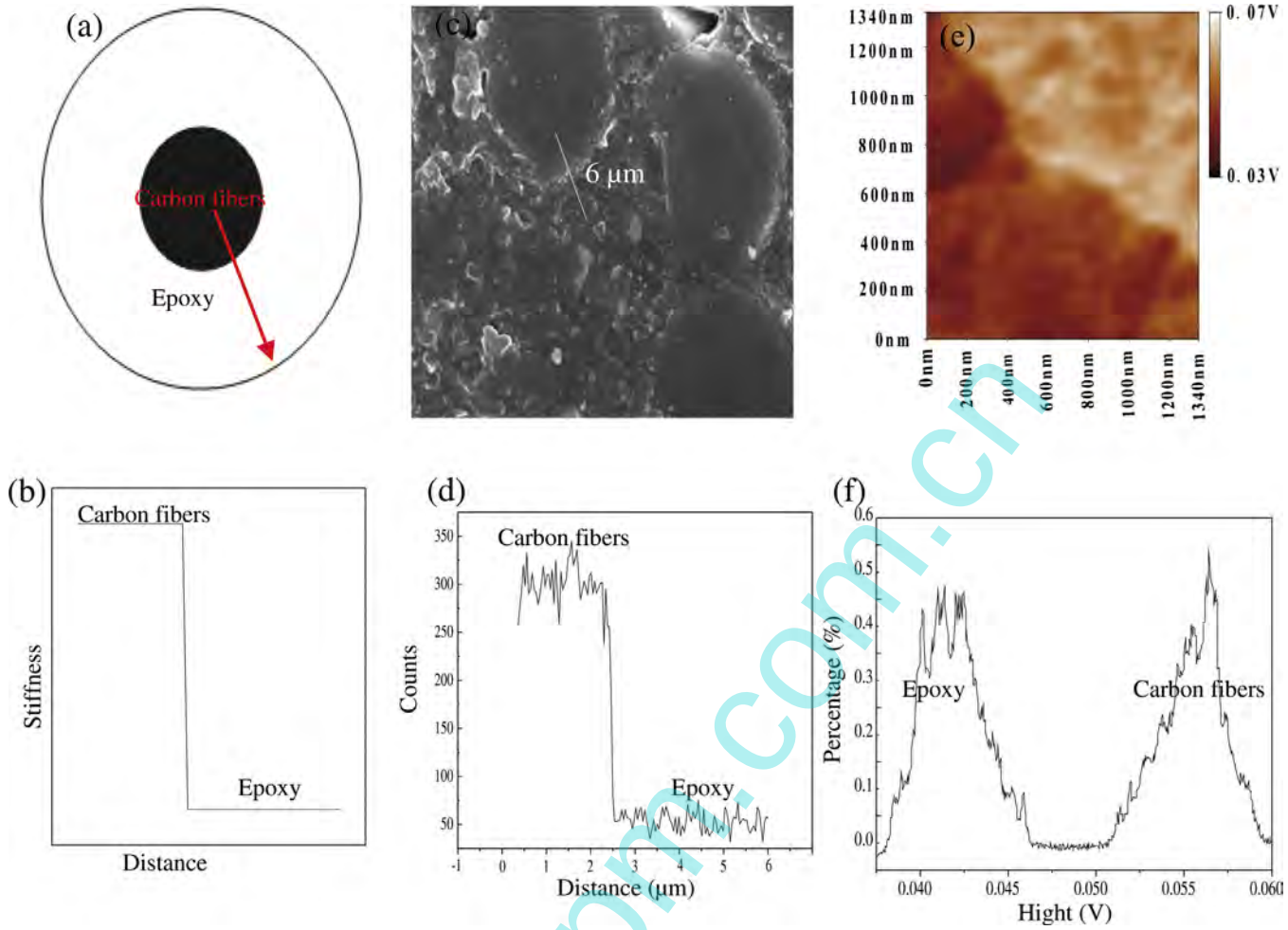

Fig. 12. (a) Illustration of the base composites. (b) Illustration of the composite stiffness along the direction of arrow in Fig. 9(a). (c) SEM of the fracture surface of base composites. (d) Carbon element content varying from carbon fibers to epoxy corresponding to Fig. 8(c). (e) Relative stiffness image of cross-section areas of the base composites. (f) Relative stiffness distribution curve of cross-section areas of the base composites corresponding to Fig. 8(e).

Fig. 12(f) denoted the relative stiffness value which was indirectly indicated by the voltage generated from the cantilever deflection of AFM, and the vertical axis denoted the percentage of the relative stiffness value. It can be seen that the stiffness distribution curve was clearly divided into two peaks in Fig. 12(f), clearly indicating that there were two stiffness phases representing carbon fibers and epoxy in the composite interface and no obvious peaks between the two peaks.

Fig. 13(a) was the illustration of hierarchical composites with 0.5 wt% SGO and Fig. 13(b) was the illustration of hierarchical composites stiffness along the direction of arrow in Fig. 12(a). Owning to the SGO/epoxy phase in the composite interface, the variation of stiffness from carbon fibers to epoxy was slower than that of base composites. Fig. 13(c) was SEM image of the fracture surface of hierarchical composites with SGO. Fig. 13(d) was the carbon element content varying from carbon fibers to epoxy corresponding to Fig. 13(c) delivered by SEM/EDS. The result showed that there was a transition of carbon element between carbon fibers and epoxy. What's more, a new stiffness phase between carbon fibers and epoxy appeared in the stiffness distribution curve of hierarchical composites with SGO, compared with the base composites, as shown in Fig. 12(f). The gradient interphase showed a moderate stiffness, which was lower than that of carbon fibers and higher than that of epoxy. Thus, the gradient interphase composed of SGO and epoxy could improve the stress distribution and transfer, and delay the crack opening in failure mode. These could ultimately lead to the improvement of ILSS and flexural properties of composites.

3.5. Reinforcement mechanism of gradient interphase

The stiffness of gradient interphase composed of nanosheets and epoxy was lower than that of carbon fibers and higher than that of epoxy. The gradient stiffness made the gradient interphase act as a stress transfer medium and the load can be transferred from epoxy to carbon fibers uniformly [20]. The small width and chemical functionality of SGO significantly altered the Van der Waals interactions among the aggregated nanofiller, making them easy to be dispersed in the epoxy. Moreover, the chemical adhesion between SGO and epoxy was enhanced due to the reaction between amino of SGO and epoxy. Therefore, the SGO/epoxy gradient interphase would improve stress transfer and delay the crack opening in failure mode. The load would be buffered and transferred from epoxy to carbon fibers uniformly. Thus, the ILSS and flexural properties of hierarchical composites with SGO were all increased. However, the ILSS and flexural properties of hierarchical

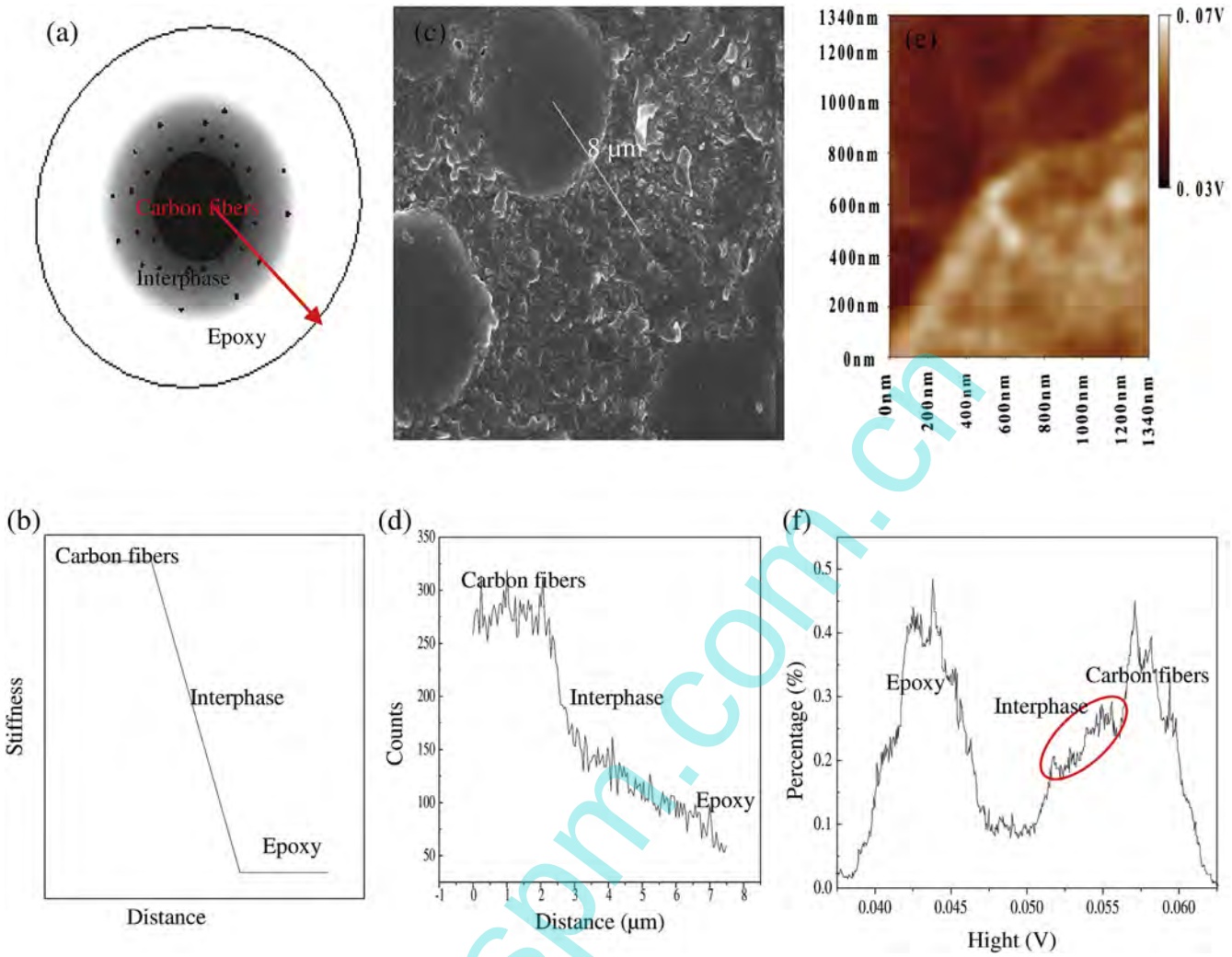

Fig. 13. (a) Illustration of the hierarchical composites with SGO. (b) Illustration of the composite stiffness along the direction of arrow in Fig. 13(a). (c) SEM of the fracture surface of hierarchical composites with SGO. (d) Carbon element content varying from carbon fibers to epoxy in the hierarchical composites with SGO corresponding to Fig. 9(c). (e) Relative stiffness image of cross-section areas of the hierarchical composites with SGO. (f) Relative stiffness distribution curve of cross-section areas of the hierarchical composites with SGO corresponding to Fig. 9(e).

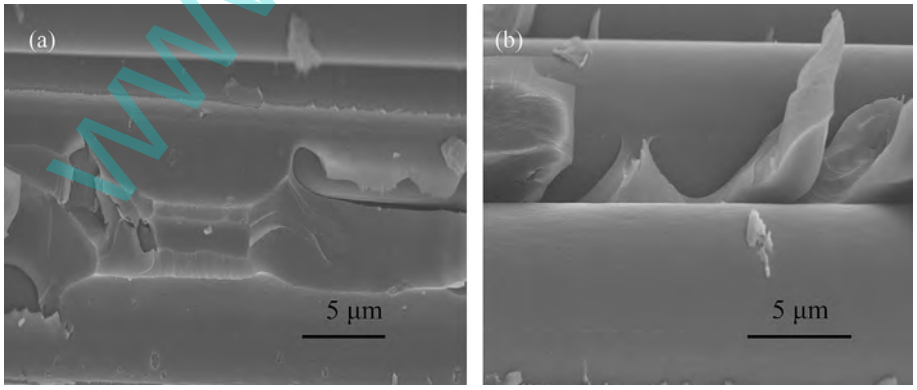

Fig. 14. (a) and (b) SEM of the fracture surface for SGO hierarchical composites and GO hierarchical composites after short beam shear tests.

composites with GO were decreased, which may be attributed to the strong tendency to aggregation and stacking in epoxy due to Van der Waals interactions [23]. In addition, the efficient chemical bonding between GO and epoxy was weak. Compared with hierarchical composites with SGO, the microstructure of GO/epoxy gradient interphase was much worse. Thus, the GO/epoxy gradient interphase would become stress concentration sites and broken firstly in failure mode.

Moreover, the resin wetting of hierarchical composites with GO was poor in comparison to hierarchical composites with SGO

during RTM. As shown in Fig. 14(b), it clearly showed the matrix detached from the fiber surface because of a weak adhesion in hierarchical composites with GO. The reason might be that the large size and morphology of GO on fibers (Figs. 1(b) and 5(f)) could reduce the surface wettability of carbon fibers during RTM.

4. Conclusions

In this study, the gradient interphase was designed in carbon/epoxy interface and confirmed by AFM in force mode and SEM/EDS successfully. The gradient interphase showed a moderate stiffness, which was lower than that of carbon fibers and higher than that of epoxy. In order to improve the dispersion of GO in gradient interphase and chemical adhesion between GO and epoxy, GO was covalently functionalizated with silane coupling agents. Compared with the base composites, the ILSS and flexural properties of hierarchical composites containing GO/epoxy gradient interphase decreased seriously. However, the IFSS, ILSS and flexural properties of hierarchical composites containing SGO/epoxy gradient interphase were all increased. Moreover, hierarchical composites containing 0.5 wt% SGO showed the highest enhancement, increasing 60% in IFSS, 19% in ILSS, 15% in flexural strength, 16% in flexural modulus and 15% in tensile strength. Consequently, a design of gradient interphase with excellent microstructure in composites will provide a promising, effective and simple method to improve the interfacial properties of composites.

Acknowledgments

The work was funded by the National Natural Science Foundation of China (U1362108, 11175130), Natural Science Foundation of Tianjin, China (10JCYBJC02300) and the National High Technology Research and Development Program of China (2012AA03A203).

References

[1] A.S. Argon, R.E. Cohen, Polymer 44 (2003) 6013–6032.
[2] X.L. Yang, Z.C. Wang, M.Z. Xu, R. Zhao, X.B. Liu, Mater. Des. 44 (2013) 74–80.
[3] J. Krysa, K. Balik, J. Krena, J. Gregor, Mater. Chem. Phys. 57 (1998) 156–161.
[4] K. Jang, W.J. Cho, C.S. Ha, Compos. Sci. Technol. 59 (1999) 995–1001.
[5] Q. Chen, L.F. Zhang, A. Rahman, Z.P. Zhou, X.F. Wu, H. Fong, Compos. Part A 42 (2007) 2036–2042.
[6] V. Kostopoulos, S. Tsantzalis, P. Karapappas, A. Vavouliotis, P. Tsotra, T. Tanimoto, K. Friedrich, Compos. Part A 38 (2007) 1159–1162.
[7] Q. Zhang, J. Liu, R. Sager, L. Dai, J. Baur, Compos. Sci. Technol. 69 (2009) 594–601.
[8] X.Q. Zhang, X.Y. Fan, C. Yan, H.Z. Li, Y.D. Zhu, X.T. Li, L.P. Yu, ACS Appl. Mater. Interfaces 4 (2012) 1543–1552.
[9] L. Mei, X. He, Y. Li, R. Wang, C. Wang, Q. Peng, Mater. Lett. 64 (2010) 2505–2508.
[10] D.C. Davis, J.W. Wilkerson, J.A. Zhu, D.O.O. Ayewah, Compos. Struct. 92 (2010) 2653–2662.
[11] C. Ren, Q.M. Gong, L.Q. Guo, X.M. Zhao, J. Liang, Micro Nano Lett. 7 (2012) 240–243.
[12] Q.Y. Peng, X.D. He, Y.B. Li, C. Wang, R.G. Wang, P.A. Hu, Y.D. Yan, T. Sritharan, J. Mater. Chem. 22 (2012) 5928–5931.
[13] B.P. Singh, V. Choudhary, P. Saini, R.B. Mathur, AIP Adv. 2 (2012) 022151.
[14] M. Tehrani, M. Safdari, A.Y. Boroujeni, Z. Razavi, S.W. Case, K. Dahmen, H. Garmestani, M.S. Al-Haik, Nanotechnology 24 (2013) 155704.
[15] F. Yavari, M.A. Rafiee, J. Rafiee, Z.Z. Yu, N. Koratkar, ACS Appl. Mater. Interfaces 2 (2010) 2738–2743.
[16] D.R. Dreyer, S. Park, C.W. Bielawski, R.S. Ruoff, Chem. Soc. Rev. 39 (2010) 228–240.
[17] S. Stankovich, D.A. Dikin, G.H.B. Dommett, K.M. Kohlhaas, E.J. Zimney, E.A. Stach, R.D. Piner, S.T. Nguyen, R.S. Ruoff, Nature 442 (2006) 282–286.
[18] P.a. Song, L. Liu, S. Fu, Y. Yu, C. Jin, Q. Wu, Y. Zhang, Q. Li, Nanotechnology 24 (2013) 125704.
[19] G.S. Wang, G.Y. Chen, Z.Y. Wei, X.F. Dong, M. Qi, Mater. Chem. Phys. 141 (2013) 997–1004.
[20] F. Zhao, Y.D. Huang, L. Liu, Y.P. Bai, L.W. Xu, Carbon 49 (2011) 2624–2632.
[21] L.T. Drzal, M.J. Rich, M.F. Koenig, P.F. Lloyd, J. Adhes. 16 (1983) 133–152.
[22] Y. Termonia, J. Mater. Sci. 25 (1990) 103–106.
[23] X. Wang, W.Y. Xing, P. Zhang, L. Song, H.Y. Yang, Y. Hu, Compos. Sci. Technol. 72 (2012) 737–743.
[24] M. Fang, K. Wang, H. Lu, Y. Yang, S. Nutt, J. Mater. Chem. 19 (2009) 7098–7105.
[25] Y. Si, E.T. Samulski, Nano Lett. 8 (2008) 1679–1682.
[26] Z. Xu, K. Xue, Nanotechnology 21 (2010) 045704.
[27] H. Xu, Z.G. Hu, A.L. Lu, Y.Y. Hu, L. Li, Y.Y. Yang, Z.Y. Zhang, H.Y. Wu, Mater. Chem. Phys. 141 (2013) 310–317.
[28] H. Yang, F. Li, C. Shan, D. Han, Q. Zhang, L. Niu, A. Ivaska, J. Mater. Chem. 19 (2009) 4632–4638.
[29] A.M. Diez-Pascual, M.A. Gomez-Fatou, F. Ania, A. Flores, J. Phys. Chem. C 116 (2012) 24193–24200.
[30] M. Munz, H. Sturm, E. Schulz, G. Hinrichsen, Compos. Part A 29 (1998) 1251–1259.
[31] D.C. Marcano, D.V. Kosynkin, J.M. Berlin, A. Sinitskii, Z. Sun, A. Slesarev, L.B. Alemany, W. Lu, J.M. Tour, ACS Nano 4 (2010) 4806–4814.
[32] S. Chengbo, C. Lei, X. Zhiwei, J. Yanan, L. Yinglin, W. Chunhong, S. Mingjing, W. Zhen, G. Qiwei, Phys. E 44 (2012) 1420–1424.
[33] S. Stankovich, D.A. Dikin, R.D. Piner, K.A. Kohlhaas, A. Kleinhammes, Y. Jia, Y. Wu, S.T. Nguyen, R.S. Ruoff, Carbon 45 (2007) 1558–1565.
[34] Y.J. Xie, C.A.S. Hill, Z.F. Xiao, H. Militz, C. Mai, Compos. Part A 41 (2010) 806–819.
[35] S.H. Shim, K.T. Kim, J.U. Lee, W.H. Jo, ACS Appl. Mater. Interfaces 4 (2012) 4184–4191.
[36] M.M. Rahman, S. Zainuddin, M.V. Hosur, J.E. Malone, M.B.A. Salam, A. Kumar, S. Jeelani, Compos. Struct. 94 (2012) 2397–2406.
[37] F. Zhihang, H. Kuang-Ting, S.G. Advani, Carbon 42 (2004) 871–876.
[38] M. Martin-Gallego, M. Hernandez, V. Lorenzo, R. Verdejo, M.A. Lopez-Manchado, M. Sangermano, Polymer 53 (2012) 1831–1838.